Self-repelling bipedal exploration process

Hor Dashti-N,[1,*] M. N. Najafi,[2,†] and Hyunggyu Park[1,‡]
[1]*School of Physics, Korea Institute for Advanced Study, Seoul 02455, Korea*
[2]*Department of Physics, University of Mohaghegh Ardabili, P.O. Box 179, Ardabil, Iran*

(Received 12 July 2021; accepted 2 November 2021; published 29 November 2021)

A self-repelling two-leg (biped) spider walk is considered where the local stochastic movements are governed by two independent control parameters β_d and β_h, so that the former controls the distance (d) between the legs positions, and the latter controls the statistics of self-crossing of the traversed paths. The probability measure for local movements is supposed to be the one for the "true self-avoiding walk" multiplied by a factor exponentially decaying with d. After a transient behavior for short times, a variety of behaviors have been observed for large times depending on the value of β_d and β_h. Our statistical analysis reveals that the system undergoes a crossover between two (small and large β_d) regimes identified in large times (t). In the small β_d regime, the random walkers (identified by the position of the legs of the spider) remain on average in a fixed nonzero distance in the large time limit, whereas in the second regime (large β_d), the absorbing force between the walkers dominates the other stochastic forces. In the latter regime, d decays in a power-law fashion with the logarithm of time. When the system is mapped to a growth process (represented by a height field which is identified by the number of visits for each point), the roughness and the average height show different behaviors in two regimes, i.e., they show a power law with respect to t in the first regime and $\log t$ in the second regime. The fractal dimension of the random walker traces and the winding angle are shown to consistently undergo a similar crossover.

DOI: 10.1103/PhysRevE.104.054135

I. INTRODUCTION

Random walks are at the heart of nonequilibrium statistical mechanics and stochastic processes. They are unique in describing nature due to their large applications in many physical systems, such as polymers in a good solvent [1], stock markets [2], thermal motion of gas molecules [3] or networks [4,5], and mathematical statistics [6]. In most cases, studies on random walks in the literature are surprisingly limited to a few cases like uncorrelated random walks, self-avoiding and loop-erased random walks [7–11], and fractional Brownian motions [12] for which the mathematical structures are more or less known. Many properties of these random walks in various dimensions have been calculated analytically and numerically. In two dimensions, we know that self-avoiding walk (SAW) is a Schramm-Loewner evolution (SLE) with a diffusivity parameter $\kappa = \frac{8}{3}$, which is consistent with a conformal field theory (CFT) with a central charge $c = 0$ [13,14], whereas a loop-erased random walk (LERW) is described by $\mathrm{SLE}_{\kappa=2}$ [15], which is consistent with the $c = -2$ CFT [16] (both CFTs are logarithmic). The former reveals a relation with the critical percolation theory [17], and the latter shows that LERW is consistent with the interfaces of sandpiles [18]. Some authors occasionally consider more sophisticated situations, like correlated random walks with dropping debris [namely, a true SAW (TSAW)] [19], self-avoiding random walks in media with quenched randomness [20], TSAW with diffusion of debris [21,22], LERW in the correlated background [23], history-dependent random walks [24–27], restricted random walks [28], and random walks on the random graphs [5,29]. Another type of correlation is the one that the motion of a random walker depends on the effective environment that is formed by the rest of the random walkers in the media. This problem applies to many systems like active matter (such as the Vicsek model of self-propelled particles [30] and active Brownian motion [31]) and thermal motion of gas molecules [3]. Polymers [32], polymer brushes [33], and traces of grains in sandpiles [34] are other examples.

In nature, there are some more sophisticated situations, such as multiagent stochastic correlated walks, which can serve as the example of few-body active dynamics, taking conditional steps depending on the structure of the background potential or effective interaction with other agents. Consider as an example two (male and female) insects that besides seeking food tend to each other and therefore perform a correlated exploration process in two dimensions, with a low tendency to step on the places where they have already stepped due to the fact that the chance of finding food in the traversed path is low. This problem can be considered as a combination of TSAW and the multiagent random walk problem, which we call a *self-repelling bipedal exploration process* (SRBP). SRBP can be taken into account as a member of a larger class, namely, the *spider walks*, defining the systems in which the particles move in such a way that their movements do not violate some given rules [35]. A DNA molecular biped on a one-dimensional walking path is another example that is mapped to a spider walk on one-dimensional [36–38] and

*hdashti@kias.re.kr
†morteza.nattagh@gmail.com
‡hgpark@kias.re.kr

two-dimensional [37] random media. There are many more examples that can be mapped to our model (SRBP as a generalization of biped spider walk) such as insect movement [39], a polymer ring entangled with obstacles [40], local clustering for multiagent random walks [41], and an animal's movement as correlated random walks [42]. Another example of the systems that can potentially be mapped to SRBP is a system with two kinds of monomers (e.g., blue and red) with an absorbing interaction between blue-red pairs and repulsion between blue-blue and red-red pairs, through the combining of which two (blue and red) self-avoiding polymers are constructed, which serves as a generalization of polymers entangled with obstacles [40].

In this paper, we consider the SRBP problem with two independent parameters, one of which controls the tendency between two agents ($\beta_d \equiv 1/T_d$), and another controls the disinclination for crossing the traversed path ($\beta_h \equiv 1/T_h$). The variables T_d and T_h can be interpreted as two different temperatures in our model. To capture the "true self-repulsion," we use the method given in [21], according to which the random walkers drop one unit of debris in the site that they are in, so that $h_i(t)$ shows the height of the debris in site i at time t. Then the random walkers come back to any site i with a probability proportional to $\exp[-\beta_h h]$ (the step length is one unit of lattice). The relative distance of two agents, the height of debris, and the random walker paths are the important quantities that we study in this paper. This system is shown to undergo anomalous diffusion (with respect to the relative coordinate) and shows a crossover point to a new phase that is determined by β_d and β_h.

The paper is organized as follows. In the next section, we introduce the model. The results for the diffusion process are presented in Sec. III. Section IV is devoted to the fractal dimension of the traces and the winding angle statistics. We close the paper with a conclusion section.

II. THE MODEL

The spider walks with k legs are defined through considering k different (coupled) traces $[X_t = (X_{1,t}, X_{2,t}, \ldots, X_{k,t}]$, where $X_{i,t}$ stands for the position of the ith leg of the spider at time t) over a given undirected connected graph $G(V, E)$ with vertex set V and edge set E. The model is identified using the transition matrix $P = \{p(x, y)\}_{x,y\in G}$, where $p(x, y)$ is zero only when the required links are missing in G. Showing the position of the spider by $\mathbf{x} = (x_1, x_2, \ldots, x_k)$, the transition to $\mathbf{y} = (y_1, y_2, \ldots, y_k)$ is given by $p(x_i, y_i)$ *if there exists exactly one index i such that* $x_i \neq y_i$. Many properties of this model have been explored in the literature, such as recurrence [35], transience, ergodicity, and spider walks in random media [35]. The example is the legs of the biped molecule (as a biped spider), which moves on the integer lattice representing the nucleic acid binding domains imprinted on the path [36].

As partially explained in the introduction, we consider two correlated random walks that step on a lattice. This problem is mapped to a generalized biped spider walk problem in the Euclidean space (square lattice). The generalization looks to the fact that the traces that are traversed by the legs of the spider matter, i.e., the traces are self-repulsive in the sense that in each time step t, the random walkers drop a unit of debris at the point that they stand on, e.g., the site i, so that the height of the site increases by one, i.e., $h_i(t) \to h_i(t) + 1$. The steps are taken according to the following update probability: Suppose that the random walkers are in points $\mathbf{r}_1^0$ and $\mathbf{r}_2^0$ at time t, and $\mathbf{r}_1$ and $\mathbf{r}_2$ are some random neighbors of $\mathbf{r}_1^0$ and $\mathbf{r}_2^0$, respectively. Then the probability to step to the neighboring sites $\mathbf{r}_1$ and $\mathbf{r}_2$ at the next time is proportional to

$$P \propto \exp\{-\beta_h[h(\mathbf{r}_1) + h(\mathbf{r}_2)]\} \exp[-\beta_d \delta d], \tag{1}$$

where $\delta d \equiv d^{\text{new}} - d^{\text{old}}$, $d^{\text{new}} \equiv |\mathbf{r}_1 - \mathbf{r}_2|$ and $d^{\text{old}} \equiv |\mathbf{r}_1^0 - \mathbf{r}_2^0|$. The first factor cares about self-repulsion, and the second one cares about the tendency between the pair, so that when both β_h and β_d are zero, all the directions are equiprobable and one retrieves two-dimensional uncorrelated random walks. The simulation is started by two agents that start from the origin. At each time the next step is taken towards a random neighbor according to the probability given above. For calculating the winding angle statistics, we prevent the agents from entering a region in a close neighborhood of the origin [43]. The larger amount of β_h leads to a smaller probability of self-intersection, so that $(\beta_d, \beta_h) \to (0, \infty)$ gives two independent ordinary SAWs. In the opposite limit for $\beta_h = 0$, and defining $d \equiv |\mathbf{r}_1 - \mathbf{r}_2|$, at long enough times, one expects that

$$\langle d \rangle = -\partial/\partial\beta_d \ln \int_0^\infty e^{-\beta_d d} dd = \beta_d^{-1} = T_d, \tag{2}$$

where the ergodicity was considered, meaning that the random walker has enough time to find any possible configuration, i.e., all d values are *visited*. The other well-known limit is $\beta_d = \beta_h = 0$, which is corresponds to two independent two-dimensional uncorrelated random walks—space filling with mass fractal dimension $d_f = 2$. The winding angle θ is defined as the total winding angle of the random walker around the origin. The general setup of the problem and the quantities of interest are schematically shown in Fig. 1, where a small region around the starting point was removed. It was shown that for the ordinary two-dimensional random walks with the starting point excluded [8,43],

$$\langle \theta^{2m} \rangle \propto (\log t)^{2m}, \tag{3}$$

and the distribution function $P_t(\theta) \propto \exp[-2\pi|\theta|\log t]$. This is in contrast to SAWs, where $\langle \theta^2 \rangle = \frac{8}{3} t$ [13]. Also, note that the characteristic distance of the random walker scales with

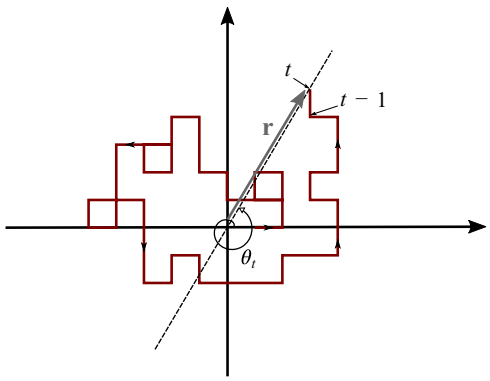

FIG. 1. Schematic representation of the random walks of one agent with the corresponding winding angle θ_t and displacement $\mathbf{r}(t)$.

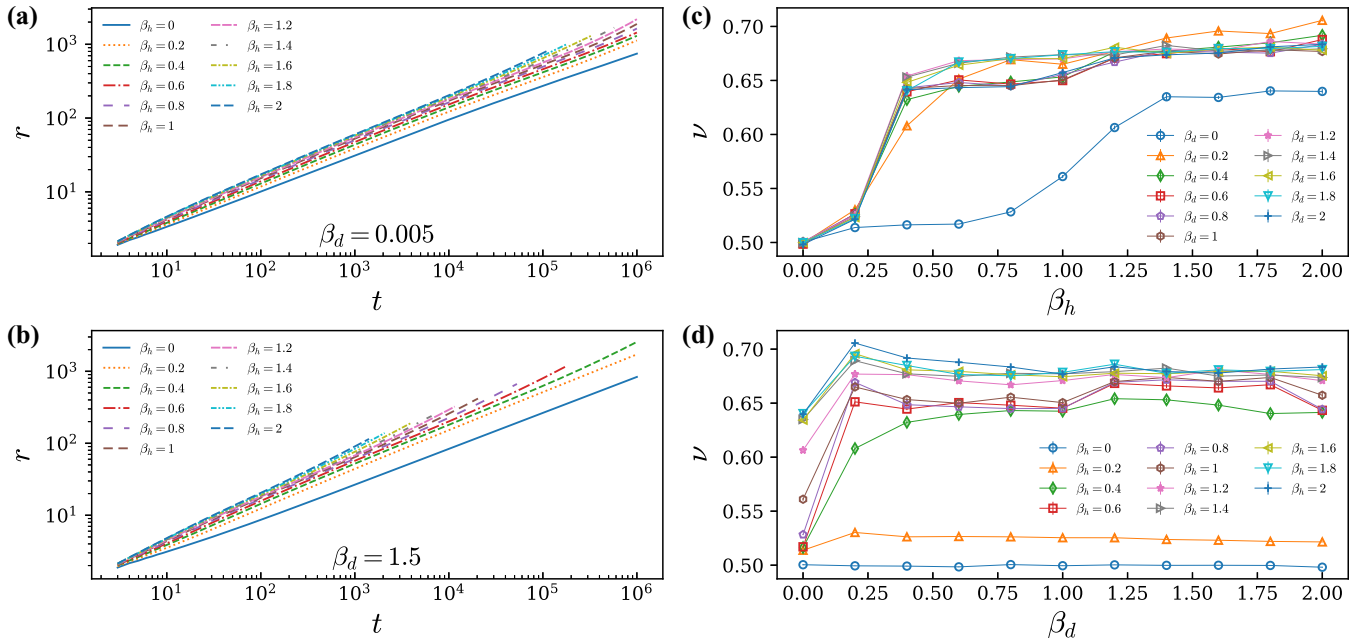

FIG. 2. Log-log plots of $r \equiv |\mathbf{r}|$ vs t for $\beta_d = 0.005$ and $\beta_d = 1.5$ for various values of β_h (each corresponding to a curve with a specific line style) are shown in (a) and (b), respectively. The slope of each curve gives the diffusion exponent ν. The corresponding exponents in terms of β_h and β_d are shown in (c) and (d), respectively. In (d) one can see that for $\beta_d \lesssim 0.2$, the diffusion exponent ν changes abruptly, and for $\beta_d \gtrsim 0.2$, it roughly remains fixed.

t^ν, where $\nu = 1/2$ for ordinary random walks and $\nu = 3/4$ for SAWs.

III. THE DIFFUSION PROCESS

In this section we present the results of the simulations. We use the Metropolis algorithm with the accepted ratio P defined in Eq. (1) to accept one of the 16 possible pair movements on a lattice at each time step t. For various values of β_d, and β_h (with variable increments), we generated more than 10^5 independent realizations, for each of which the time runs up to $t = 10^6$. The run time for high β_h values increases dramatically because of the self-avoiding character of the traces.

The type of diffusion (normal, sub-, and superdiffusion) for each agent is arguably the most important question in the transport perspective. Our inspections show that the statistics of the random walkers are quite sensitive to β_d and β_h. Importantly, the position of each random walker $r \equiv |\mathbf{r}|$ crosses over from normal diffusion (identified by an exponent $\nu = \frac{1}{2}$ in the scaling relation $r \propto t^\nu$) to a regime with a different diffusion exponent; see Fig. 2. As β_h increases, one expects that the SAW behavior is retrieved, $\nu^{\mathrm{SAW}} = \frac{3}{4}$ [13], which is expected from Fig. 2(c), while the dependence on β_d is quite low for $\beta_d \gtrsim 0.2$. As β_d increases, the crossover to the new regime happens earlier, i.e., β_d facilitates this crossover.

The relative distance between the random walkers ($d_{\beta_d,\beta_h}(t)$) is the other quantity that shows considerable change as β_d and β_h vary. Figure 3 shows this quantity in terms of time t for various amounts of β_h and for $\beta_d = 0.2$ and 2 [Figs. 3(a) and 3(b) respectively]. For both cases in the early times, the distance between the random walkers (agents) increases with time in a power-law fashion. There is, however, an important difference between them in long times: for $\beta_d = 0.2$ the graph saturates to a β_h-dependent constant, while the graph for $\beta_d = 2$, d decays in a power-law fashion *in terms of* $\log t$. More precisely, in the large β_d regime, the random walkers are asymptotically absorbed to each other with a heavy tail function:

$$d^{\mathrm{R2}}_{\beta_d,\beta_h}(t)\big|_{\text{large times}} \propto (\log t)^{-\alpha_d}. \tag{4}$$

Our observations show that a crossover is established between two distinct regimes in terms of β_d identified by different statistical behaviors. Let us show the crossover region by β_d^*, which is [0.2, 0.5]. For β_d smaller than β_d^* (let us call it the R1 regime), d saturates to a constant value for long enough times [like $\beta_d = 0.2$ in Fig. 3(a)], while for $\beta_d > \beta_d^*$ (the R2 regime) d varies in the form of Eq. (4) [like $\beta_d = 2$ in Fig. 3(b)]. For the R1 regime, the curves for d are collapsed (fitted to each other) with an appropriate choice of exponents, a fact that was not observed for the R2 regime. Figures 3(c) and 3(d) show the data collapse analysis for the R1 regime for $\beta_h = 0.2$ and 1, demonstrating that the relative distance of the agents satisfies the following scaling behavior (for all β_h values in the interval [0.01, 1]; also note that it is not applicable for R2 regime):

$$d^{\mathrm{R1}}_{\beta_d,\beta_h}(t) = C(\beta_h)\beta_d^{-b} F\left(\beta_d^a t\right), \tag{5}$$

where a and b are their corresponding exponents, $C(\beta_h)$ is a smooth function of β_h, and F is a universal function with the asymptotic behavior $\lim_{x\to 0} F(x) \propto x^{b/a}$ and $\lim_{x\to\infty} F(x) =$ const. These exponents are interestingly more or less independent of β_h for $\beta_h \in [0.01, 1]$, being fixed at $a = 2.00 \pm 0.05$ and $b = 1.00 \pm 0.05$. This shows that $d(t)_{\text{small times}} \propto t^z$ where the dynamic exponent $z = 0.51 \pm 0.02$ lies pretty much within the normal diffusion regime. We notice that this

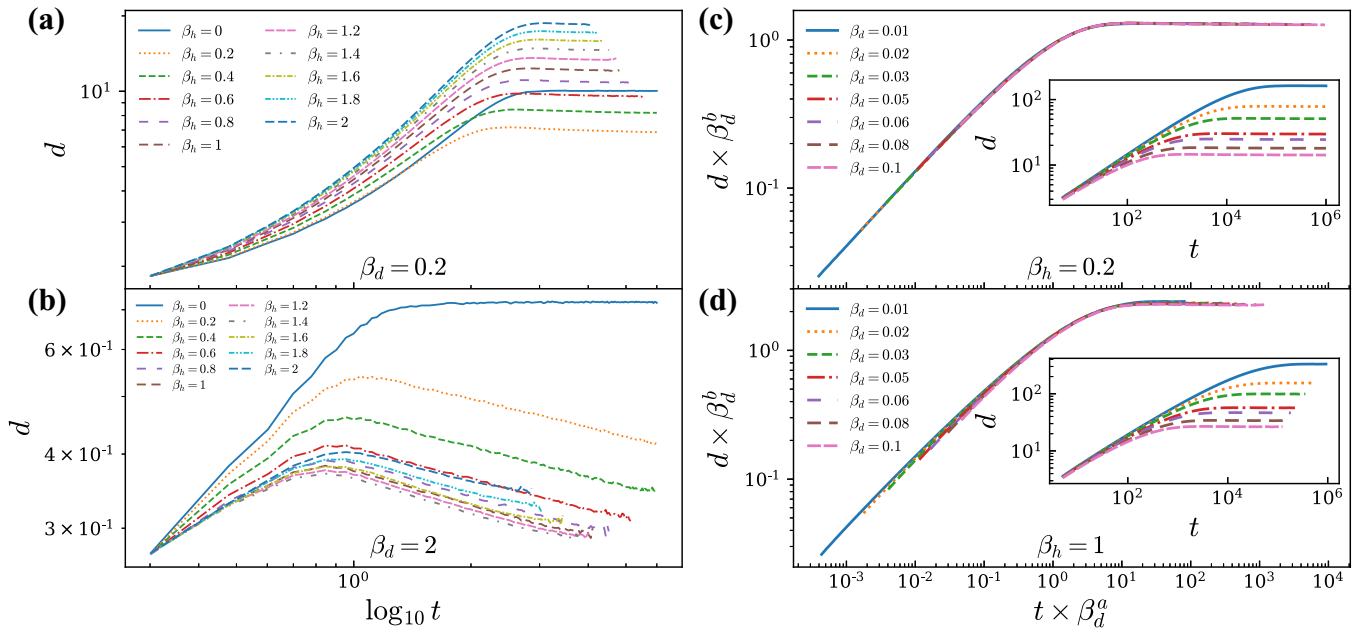

FIG. 3. Log-log plots of $d \equiv |\mathbf{r}_1 - \mathbf{r}_2|$ in terms of $\log_{10} t$ for $\beta_d = 0.2$ and for $\beta_d = 2$ are plotted in (a) and (b), respectively. It is clear that we have two different behaviors in (a) and (b). The $\beta_d = 0.2$ and $\beta_d = 2$ belong to the R1 and R2 regimes, respectively. When $\beta_h \approx 0$, these differences do not exist anymore; i.e., the variable $d(t)$ reaches a saturation value d_s at a big enough time for all values of $\beta_d > 0$. The corresponding data collapse analysis for $\beta_h = 0.2$ and $\beta_h = 1$ with $a = 2.00(5)$ and $b = 1.00(5)$ is shown in (c) and (d), respectively. It is worth noting that the data collapse happens in the R1 regime ($\beta_h > 0$, $\beta_d \lesssim 0.2$).

behavior cannot be valid for (or simply extrapolated to) much larger β_h where one expects the SAW regime with $z_{\text{SAW}} = \frac{3}{4}$.

To monitor the differences of the R1 and R2 regimes, we show the α_d exponent in terms of β_d and β_h in Figs. 4(a) and 4(b), respectively. α_d is almost zero for $\beta_d \lesssim 0.6$ [inset of Fig. 4(a)] as expected from the definition of the R1 regime and grows more or less linearly by increasing β_d starting from $\beta_d \approx 0.6$, consistent with the above claim ($\beta_h = 0$ is an exception for which α_d is almost zero everywhere). The dependence of α_d on β_h is low [Fig. 4(b)], as can also be seen in the other observables like Fig. 5 where d_s is the amount of d at a fixed time $t = 10^3$ after the saturation is established. The latter figure shows that the change of d_s with respect to β_h is negligibly small. For small β_d values, the graphs are fitted with the relation $d_s \propto 1/\beta_d$, which is true for all β_h values considered in this work [in agreement with Eqs. (2) and (5)], while some deviations are observed for large β_d values.

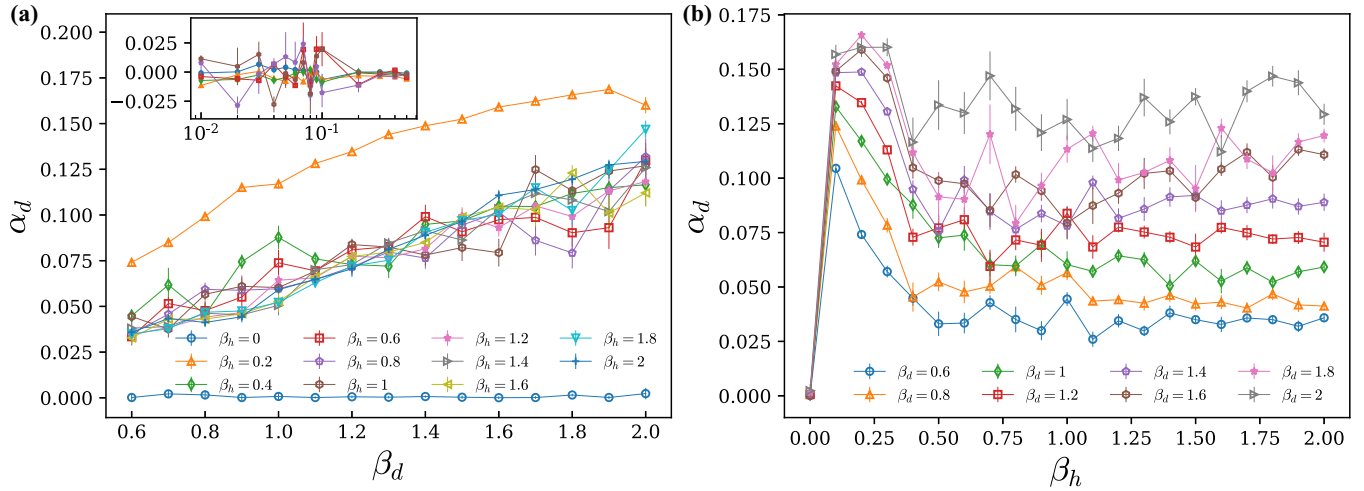

FIG. 4. The exponents α_d in terms of β_d for $0.5 < \beta_d < 2$, and $0 < \beta_d \leqslant 0.5$ are shown in the main panel and inset of (a), respectively. In the two mentioned regimes, R1 and R2, we see different behaviors for $d(t) = |\mathbf{r}_1 - \mathbf{r}_2|$. In the first regime, $d(t)$ reaches a plateau region. But in the second regime, we see $d(t)$ follows the power law in terms of $\log_{10} t$. The legend of the inset figure is the same as the main panel. The x-axis of the inset is in $\log_{10}$ scale for making the graph clearer. In (b) the exponent α_d is plotted in terms of β_h, which roughly remains fixed for almost large β_h.

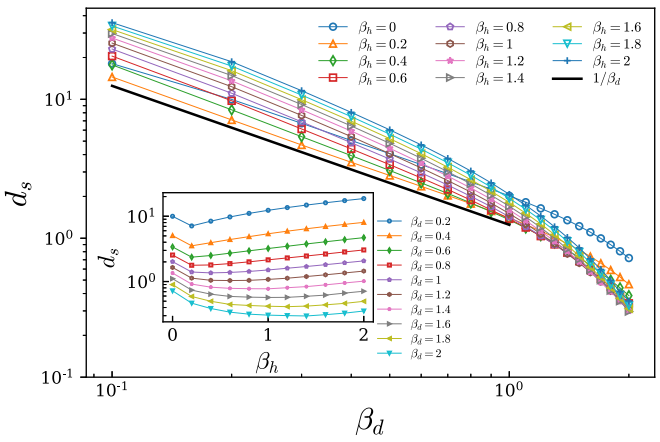

FIG. 5. The amount of d at $t = 10^3$ in terms of β_d for various values of β_h is shown in main panel. For small values of β_d, $d(t)$ reaches d_s, and all curves follow the scaling relation $d_s \propto 1/\beta_d$, which is consistent with Eq. (2). The change of d_s with respect to β_h for each curve (corresponding to a β_d), is negligibly small, which is shown in the inset.

The problem of random walkers in two dimensions can readily be mapped to a (2+1)-dimensional growth by considering the statistics of the height produced by the amount of debris left by random walkers at each site. There is considerable literature on mapping a landscape generated by debris in TSAW to rough surfaces. In the original paper by Amit *et al.* [19], it was assumed that the roughness can be neglected, so that the rough surface is characterized only by its gradient. Obukhov and Peliti then argued that roughness is a significant quantity as well as the gradient [44]. This was further discussed by Derkachov *et al.* [45]. Whatever the correct description of the landscape, it is characterized by long-range correlations. From this point of view, the roughness is arguably the significant quantity that identifies the system's universality class. It is defined by

$$w^2 = \langle \overline{(h(\mathbf{r}) - \bar{h})^2} \rangle, \tag{6}$$

where the overbar represents the spatial average $\overline{O} \equiv \frac{1}{m(t)} \sum_{x,y \in \Gamma(t)} O(x,y)$, and $\langle \cdots \rangle$ is the ensemble average. The variables $m(t) = \sum_i \Theta(h_i(t) - 1)$ and $\Gamma(t)$ are the number of occupied sites and the set of all occupied sites, respectively. Also, Θ is the step function defined by $\Theta(x) = 1$ for $x \geqslant 0$ and zero otherwise. We found a same crossover point in terms of t, so that for $\beta_d \ll \beta_d^*$ (R1 regime) both h ($=\langle \bar{h} \rangle$) and w grow with time in a power-law fashion, while for $\beta_d \gg \beta_d^*$ (R2 regime) both of them grow with a power of $\log t$. For $\beta_d \approxeq \beta_d^*$ both behaviors are observed, one for small timescales and another for large times.

Two extreme cases (R1 and R2 regimes) for w have been shown in Fig. 6 (the results for h are quite similar to w, which can be realized from scaling arguments). Figures 6(a) and 6(b) are w^2 for $\beta_d = 0.005$ (in the R1 regime) and $\beta_d = 1.5$ (in the R2 regime) respectively, from which we see that the log-log plot of roughness is linear with time in the R1 regime, whereas it is linear with respect to $\log t$ in the R2 regime. The quantities shown in Figs. 6(c) and 6(d) are the corresponding exponents in long times defined by

$$w^2_{\mathrm{R1}} \propto t^{\alpha_w^{(1)}}, \quad w^2_{\mathrm{R2}} \propto (\log t)^{\alpha_w^{(2)}}. \tag{7}$$

It should be noted that the label and the scale of the axes in Figs. 6(a) and 6(b) have been chosen in accordance with the fact that Fig. 6(a) describes the R1 regime and satisfies the first

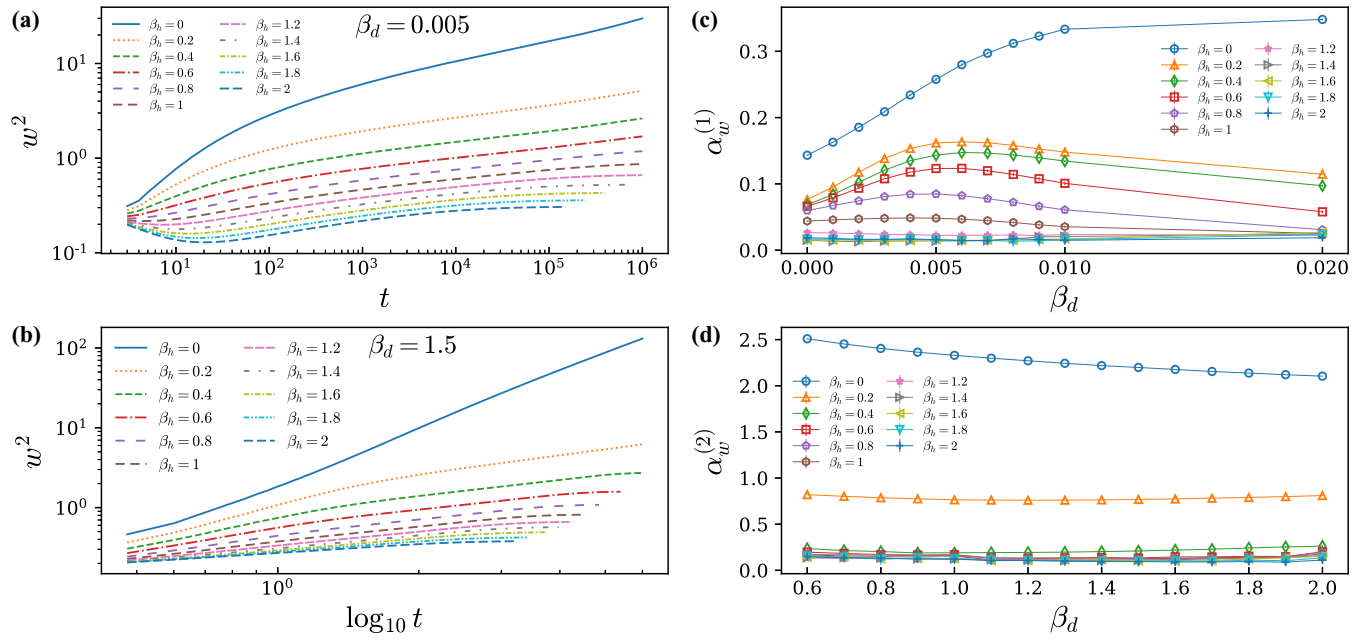

FIG. 6. Log-log plot of w^2 in terms of t for $\beta_d = 0.005$ is plotted in (a). This β_d is found in the R1 regime, in which the width is proportional to $t^{\alpha_w^{(1)}}$. In (b) the log-log plot of width is shown in terms of $\log_{10} t$ for $\beta_d = 1.5$. This β_d belongs to the R2 regime, in which $w^2(t) \propto (\log t)^{\alpha_w^{(2)}}$. In (c) and (d), the exponents $\alpha_w^{(1)}$, and $\alpha_w^{(2)}$ are depicted in terms of β_d in the regions $\beta_d \ll 0.2$ and $\beta_d \gg 0.2$ for various amounts of β_h, respectively.

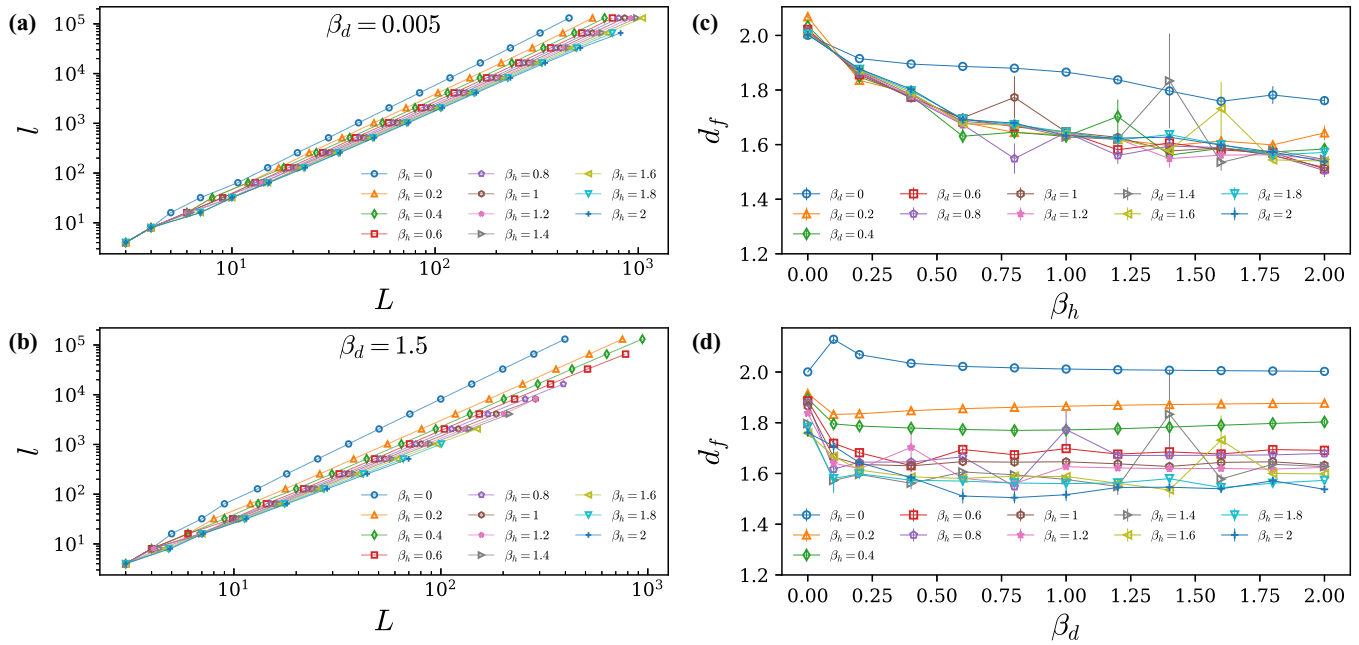

FIG. 7. Log-log plots of trace length of the random walker (l) in terms of L (lateral size of minimal square containing the whole trace) for $\beta_d = 0.005$ and $\beta_d = 1.5$ are shown in (a) and (b), respectively. The slope of each curve yields the fractal dimension d_f of random walker traces. The corresponding fractal dimensions calculated using the sandbox method in terms of β_h and β_d are shown in (c) and (d), respectively. In (d) one can see that for $\beta_d \lesssim 0.2$, the value of d_f changes abruptly. But for $\beta_d \gtrsim 0.2$, the value of d_f remains almost fixed.

relation of the above equation. In contrast, Fig. 6(b) belongs to the R2 regime and satisfies the second relation.

Considering Figs. 6(c) and 6(d), we see that $\alpha_w^{(1)}$ after a slight increase shows a decreasing behavior in terms of β_d (it decreases with β_h), while $\alpha_h^{(2)}$ is more or less constant. Both exponents decrease with β_h for all β_d values. $\alpha_w^{(1)}$ is not a monotonic function in terms of β_d, showing a maximum at $\beta_d \approx 0.005$, while it decreases with β_h confirming that it is entering a logarithmic regime. $\alpha_w^{(2)}$ is almost robust against β_d and decreases with β_h. Note that our definition of spatial averaging differs from the one used in [21] (here the average is over the occupied sites), so that our exponents cannot be compared with that paper. We are not sure whether this behavior of the roughness remains unchanged as $t \to \infty$ or it enters a stationary regime, for which much larger scale simulations are needed. The second way out of this problem might be to consider the random walkers on a finite lattice, which is beyond the scope of this paper.

IV. FRACTAL PROPERTIES

The comparison of the fractal properties of the random walker traces with the other known exact results reveals the properties of the model. It especially helps significantly to understand the nature of the crossover. We have used the sandbox method [46] to estimate the fractal dimension (FD). There are many other methods for estimating the fractal FD, like box counting, gyration radius, etc., that should be the same in the scaling limit, i.e., $L \to \infty$. But for finite systems, the estimated FD and the data quality depend on the chosen method. Briefly, one considers the traces for one random walker up to time t with length $l(t)$ and encloses it with a minimal square with an edge length L. The scaling relation between l and L gives us the FD, $l(t) \sim L(t)^{d_f}$. In Figs. 7(a) and 7(b), this relation is shown for the R1 and R2 regimes, respectively. The exponent d_f can be considered as the dynamical mass FD since the quantities are time dependent. We calculate the effective d_f in terms of β_h and β_d [Figs. 7(c) and 7(d), respectively]. The FD of $\beta_d = \beta_h = 0$ is almost 2 as expected for two-dimensional uncorrelated random walks. Note also that the other extreme is $\beta_h \to \infty$ for which $d_f^{\mathrm{SAW}} = \frac{4}{3}$. From Fig. 7(c) we see that FD decreases as β_h increases (showing that the traces become sparse), approaching this value. Figure 7(d) shows that for $\beta_d > \beta_d^*$, FD becomes almost constant in terms of β_d.

Now we are in the position to test the statistics of the winding angle defined in Fig. 1. Its variance $\langle\theta^2\rangle$ is given in Eq. (3) for $\beta_d = \beta_h = 0$. This function is linear in the log-log scale plot in terms of $\log_{10} t$ shown in Figs. 8(a) and 8(b) with the exponents in large timescales given in Figs. 8(c) and 8(d). These results confirm that Eq. (3) is applicable for all cases with generalized exponents; i.e., it should be generalized to

$$\langle\theta^2\rangle = A(\log t)^{\alpha_\theta(\beta_d,\beta_h)}, \quad \alpha_\theta(0,0) = 2, \tag{8}$$

where A is a nonuniversal constant. From Figs. 8(c) and 8(d), one observes that α_θ changes from 2 to the lower values. It is hard to decide whether this exponent is identical for all β_d and β_h values when β_h is high enough. Roughly speaking, α_θ changes from 2 for small β_h and β_d values to $0.9 < \alpha_\theta(\beta_d, \beta_h) < 1.2$ for large β_h and β_d.

It is interesting to note that there is a universal point t^* where for a fixed β_d all the graphs for various β_h meet each other. The slope of the graphs is different on two sides of this point, so that t_θ^* is served as the crossover point between small- and large-scale behaviors. We calculate α_θ by

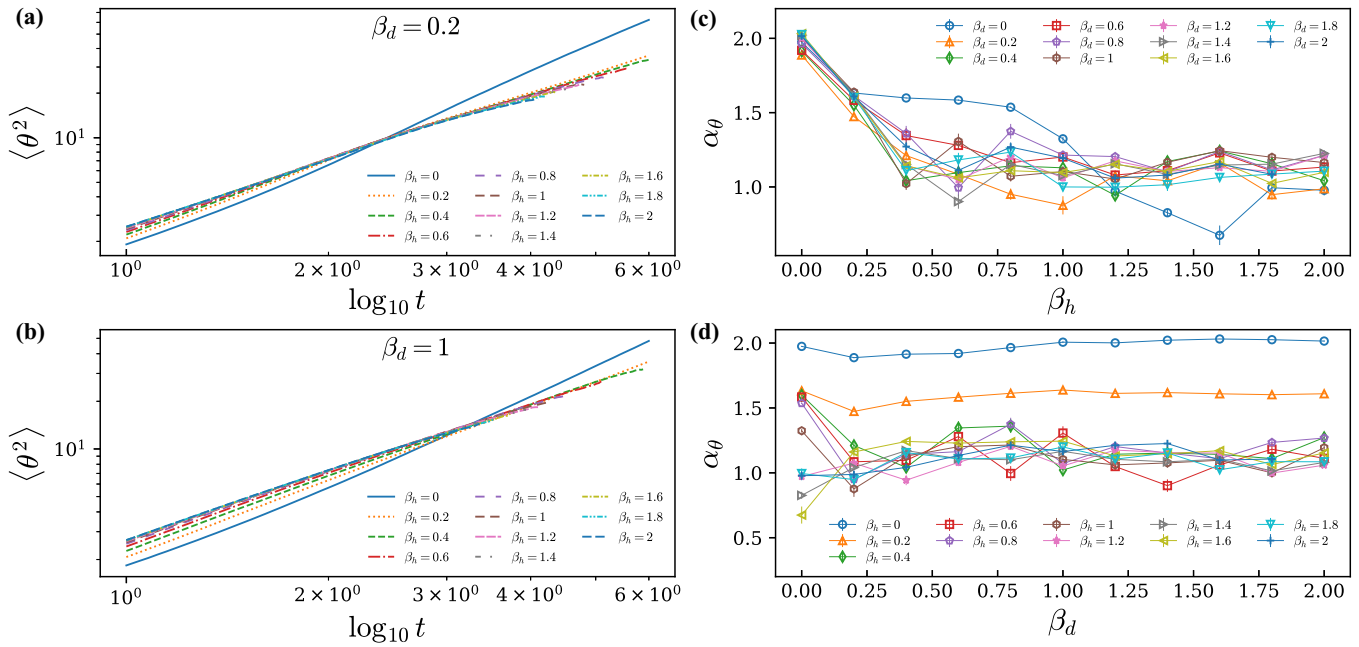

FIG. 8. Log-log plots of the variance of the winding angle $\langle\theta^2\rangle$ in terms of $\log_{10} t$ for $\beta_d = 0.2$ and $\beta_d = 1$ are shown in (a) and (b), respectively. Panels (a) and (b) have the same legend. The slope of each curve in the significant times gives α_θ. It seems that all curves in each panel meet at a specific time, e.g., t^*. We show the dependency of t_* on β_d in Fig. 9. The corresponding exponent α_θ in the long-time limit in terms of β_h and β_d is plotted in (c) and (d), respectively. For $\beta_d \lesssim 0.2$ in (d), one can see that the value of d_f changes abruptly. But for $\beta_d \gtrsim 0.2$, the value of α_θ almost remains fixed.

extracting the slopes on the right-hand side of this point, i.e., large timescales. Using this fact, one can conclude that A must follow $A = C/(\log t_\theta^*)^{\alpha_\theta(\beta_d,\beta_h)}$, where C is a nonuniversal constant, reading

$$\langle\theta^2\rangle = C\left(\frac{\log t}{\log t_\theta^*}\right)^{\alpha_\theta(\beta_d,\beta_h)}. \tag{9}$$

To calculate t_θ^*, we identify the crossing point of each two curves corresponding to different values of β_h. The reported t_θ^* is the average value, and the error bar is the variance of it.

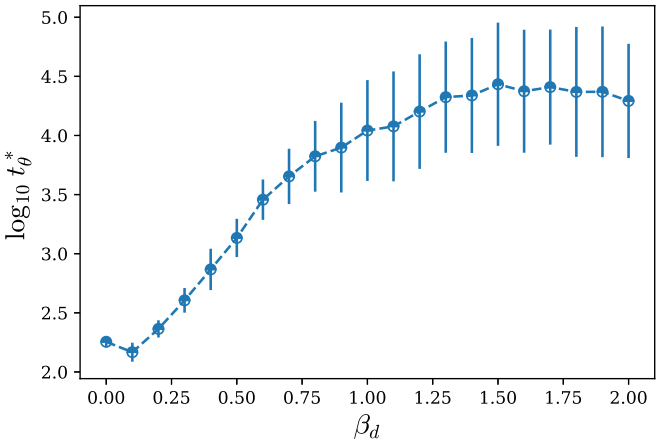

FIG. 9. The crossover time t_θ^* related to $\langle\theta^2\rangle$ curves [see Eq. (9) and Fig. 8] in terms of β_d is shown. It seems that for $\beta_d < 0.2$, the value of t^* decreases. But for $\beta_d > 0.2$, it increases, and finally for large β_d greater than 0.5, the values of t_θ^* roughly remain fixed within the error bar.

Figure 9 shows $\log_{10} t_\theta^*$ in terms of β_d, in which we see that it changes behavior when one crosses from the R1 regime to R2 regime, i.e., in the R1 regime it is an increasing function of β_d, while for the R2 regime it almost saturates to a constant.

V. CONCLUSION

This paper is devoted to the analysis of a biped spider walk, i.e., two correlated self-repelling random walkers, which is realized by dropping debris in the lattice points that are visited. The motion of random walkers is controlled by two external parameters (β_d, β_h) where β_d captures the tendency of the random walkers to each other, and β_h controls the possibility that a random walker steps on a site with debris height h. As an assessment of our model, we checked the following limits:

$(\beta_d, \beta_h) \to (0, 0)$, which is simple random walk with the fractal dimension $d_f = 2$ corresponding to the diffusion exponent $\nu = 1/2$. Also, the second moment of the winding angle is expected to show a power-law behavior with $\log t$ [see Eq. (8)].

$(\beta_d, \beta_h) \to (\text{finite}, 0)$, where the stationary distance between random walkers is expected to behave like Eq. (2).

In the limit $(\beta_d, \beta_h) \to (0, \infty)$, our model is expected to behave like SAWs, for which we have observed compatible results.

Our study uncovers the fact that there is a crossover point in which random walkers change from uncorrelated random walks to a regime that is characterized in this paper in detail. In the regime, the system is in the superdiffusion phase with some diffusion exponents higher than $\frac{1}{2}$. By analyzing the diffusion exponent and the fractal dimension of the random walker traces, we showed that regime although exhibiting

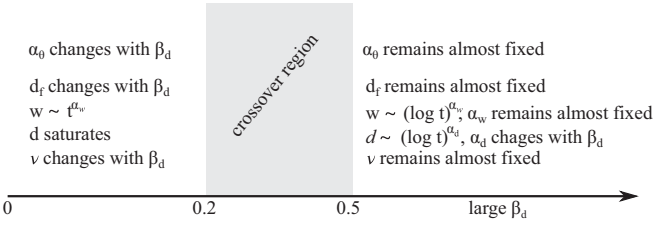

FIG. 10. We summarize the important findings of the paper. Our significant finding is the crossover behavior in terms of β_d. This crossover region is $\beta_d^* \in [0.2 - 0.5]$. Moreover, for case $(\beta_d, \beta_h) \to (0, 0)$, the system behaves like two independent random walks. When $(\beta_d, \beta_h) \to (0, \infty)$, we expect two independent ordinary self-avoiding random walks. For large values of β_h, the exponents of α_d, α_θ remain almost unchanged.

properties partially similar to self-avoiding walks represents unique features. The first regime which is identified by a crossover region $\beta_d \lesssim \beta_d^* \in [0.2 - 0.5]$ (β_d^* is a crossover point) is called the R1 regime, whereas the other regime is called R2.

In the long-time limit, the random walkers stay in a finite equilibrium distance in the R1 regime, while they tend to stay near each other in R2 regime. This tendency is described by a power-law decay of $d = |\mathbf{r}_1 - \mathbf{r}_2|$ in terms of the logarithm of time. The decay is faster for lower β_d [Fig. 4(a)], while it is not very sensitive to β_h (for not very small β_h).

A similar crossover is seen for the sandbox fractal dimension of random walker traces, which is expected to become an uncorrelated random walk $d_f^{\mathrm{URW}} = 2$ as $(\beta_d, \beta_h) \to (0, 0)$, and SAW as $(\beta_d, \beta_h) \to (0, \infty)$ with $d_f^{\mathrm{SAW}} = \frac{4}{3}$. We observed that the traces become more sparse (more self-avoiding) as β_h increases, i.e., d_f, starting from 2 (the uncorrelated case) decreases with β_h saturating to a value. For $\beta_d \neq 0$ this final fractal dimension is almost independent of β_d; e.g., it is 1.6 ± 0.1 for $\beta_h = 2.0$.

In the analysis of the winding angle, two important facts were found: (1) the variance of the winding angle regarding Eq. (3) with a different exponent [Eq. (9)] which is not effectively β_d-dependent, and is pretty sensitive to β_h (transiting from 2.0 ± 0.1 to 1.1 ± 0.2) and (2) there is a crossover time t_θ^* where for fixed β_d all the β_h graphs meet each other almost in a same point. We observed that the slopes of the graphs before and after this point are slightly different (Fig. 8). The important findings of the paper are summarized in Fig. 10.

ACKNOWLEDGMENTS

H.D.N. is supported by a KIAS Individual Grant No. PG066902 at the Korea Institute for Advanced Study. H.P. is supported by a KIAS Individual Grant No. PG013604 at the Korea Institute for Advanced Study. This work is supported by the Center for Advanced Computation at KIAS. We thank Peter Grassberger for illuminating discussions.

[1] P.-G. De Gennes and P.-G. Gennes, *Scaling Concepts in Polymer Physics* (Cornell University Press, Ithaca, NY, 1979).
[2] M. F. Osborne, Brownian motion in the stock market, Oper. Res. **7**, 145 (1959).
[3] R. Tsekov, Brownian motion of molecules: A stochastic approach, Ann. Univ. Sofia Fac. Chem. **88**, 67 (2000).
[4] C. Avin and B. Krishnamachari, The power of choice in random walks: An empirical study, in *Proc. 9th ACM Intl. Symp. on Modeling Analysis and Simulation of Wireless and Mobile Systems* (Association for Computing Machinery, Terromolinos, Spain, 2006), pp. 219–228.
[5] S. P. Boyd, A. Ghosh, B. Prabhakar, and D. Shah, Mixing times for random walks on geometric random graphs, in *Proceedings of the Seventh Workshop on Algorithm Engineering and Experiments and the Second Workshop on Analytic Algorithmics and Combinatorics, ALENEX/ANALCO*, edited by C. Demetrescu, R. Sedgewick, and R. Tamassia (SIAM, Vancouver, 2005), pp. 240–249.
[6] F. Spitzer, *Principles of Random Walk*, Vol. 34 (Duke University Press, Durham, North Carolina, United States, 2013).
[7] G. F. Lawler, A self-avoiding random walk, Duke Math. J. **47**, 655 (1980).
[8] J. Rudnick and Y. Hu, The winding angle distribution of an ordinary random walk, J. Phys. A: Math. Gen. **20**, 4421 (1987).
[9] G. F. Lawler, Loop-erased random walk, *Perplexing Problems in Probability Festschrift in Honor of Harry Kesten*, edited by M. Bramson and R. Durrett (Birkhäuser Boston, Boston, MA, 1999), pp. 197–217.
[10] M. Bauer, D. Bernard, and K. Kytölä, LERW as an example of off-critical SLEs, J. Stat. Phys. **132**, 721 (2008).
[11] R. Sepehrinia, A. A. Saberi, and H. Dashti-Naserabadi, Random walks on intersecting geometries, Phys. Rev. E **100**, 022144 (2019).
[12] J. Beran, *Statistics for Long-Memory Processes*, Monographs on Statistics and Applied Probability Series, Vol. 61 (CRC Press, Boca Raton, FL, 1994).
[13] J. Cardy, SLE for theoretical physicists, Ann. Phys. **318**, 81 (2005).
[14] A. A. Saberi, H. Dashti-Naserabadi, and S. Rouhani, Classification of $(2 + 1)$-dimensional growing surfaces using Schramm-Loewner evolution, Phys. Rev. E **82**, 020101(R) (2010).
[15] O. Schramm, Scaling limits of loop-erased random walks and uniform spanning trees, Isr. J. Math. **118**, 221 (2000).
[16] S. Majumdar and D. Dhar, Equivalence between the Abelian sandpile model and the $q \to 0$ limit of the Potts model, Physica A **185**, 129 (1992).
[17] P. Mathieu and D. Ridout, From percolation to logarithmic conformal field theory, Phys. Lett. B **657**, 120 (2007).
[18] A. A. Saberi, S. Moghimi-Araghi, H. Dashti-Naserabadi, and S. Rouhani, Direct evidence for conformal invariance of avalanche frontiers in sandpile models, Phys. Rev. E **79**, 031121 (2009).
[19] D. J. Amit, G. Parisi, and L. Peliti, Asymptotic behavior of the "true" self-avoiding walk, Phys. Rev. B **27**, 1635 (1983).
[20] P. Grassberger, Recursive sampling of random walks: Self-avoiding walks in disordered media, J. Phys. A: Math. Gen. **26**, 1023 (1993).

[21] P. Grassberger, Self-Trapping Self-Repelling Random Walks, Phys. Rev. Lett. **119**, 140601 (2017).
[22] P. Grassberger, How fast does a random walk cover a torus? Phys. Rev. E **96**, 012115 (2017).
[23] J. Cheraghalizadeh and M. Najafi, Correlation effects in the diluteness pattern in non-integral dimensional systems on superdiffusion process, Phys. Scr. **94**, 095204 (2019).
[24] R. Dickman and D. ben Avraham, Continuously variable survival exponent for random walks with movable partial reflectors, Phys. Rev. E **64**, 020102(R) (2001).
[25] R. Dickman, F. Fontenele Araujo, Jr., and D. ben Avraham, Asymptotic analysis of a random walk with a history-dependent step length, Phys. Rev. E **66**, 051102 (2002).
[26] R. Dickman, F. F. Araujo Jr., and D. Ben-Avraham, Variable survival exponents in history-dependent random walks: Hard movable reflector, Braz. J. Phys. **33**, 450 (2003).
[27] J. Marro and R. Dickman, *Nonequilibrium Phase Transitions in Lattice Models* (Cambridge University Press, Cambridge, 2005).
[28] M. N. Barber, N. Nakanishi, B. Ninham, and B. Ninham, *Random and Restricted Walks: Theory and Applications* (Gordon & Breach, New York, 1970).
[29] N. Craswell and M. Szummer, Random walks on the click graph, in *Proc. 30th Annual Intl. ACM SIGIR Conf. on Research and Development in Information Retrieval* (Association for Computing Machinery, Amsterdam, The Netherlands, 2007), pp. 239–246.
[30] H. Chaté, F. Ginelli, G. Grégoire, F. Peruani, and F. Raynaud, Modeling collective motion: Variations on the Vicsek model, Eur. Phys. J. B **64**, 451 (2008).
[31] G. Volpe, S. Gigan, and G. Volpe, Simulation of the active Brownian motion of a microswimmer, Am. J. Phys. **82**, 659 (2014).
[32] M. E. Fisher, Shape of a self-avoiding walk or polymer chain, J. Chem. Phys. **44**, 616 (1966).
[33] S. T. Milner, Polymer brushes, Science **251**, 905 (1991).
[34] M. Najafi, Z. Moghaddam, M. Samadpour, and N. A. Araújo, Invasion sandpile model, J. Stat. Mech. (2020) 073205.
[35] C. Gallesco, S. Müller, and S. Popov, A note on spider walks, ESAIM: Probab. Stat. **15**, 390 (2011).
[36] T. Antal, P. L. Krapivsky, and K. Mallick, Molecular spiders in one dimension, J. Stat. Mech. (2007) P08027.
[37] T. Antal and P. L. Krapivsky, Molecular spiders on a plane, Phys. Rev. E **85**, 061927 (2012).
[38] I. Ben-Ari, K. Boushaba, A. Matzavinos, and A. Roitershtein, Stochastic analysis of the motion of DNA nanomechanical bipeds, Bull. Math. Biol. **73**, 1932 (2011).
[39] P. Kareiva and N. Shigesada, Analyzing insect movement as a correlated random walk, Oecologia **56**, 234 (1983).
[40] A. Grosberg and H. Frisch, Winding angle distribution for planar random walk, polymer ring entangled with an obstacle, and all that: Spitzer–Edwards–Prager–Frisch model revisited, J. Phys. A: Math. Gen. **36**, 8955 (2003).
[41] M. Alamgir and U. Von Luxburg, Multi-agent random walks for local clustering on graphs, in *Proc. 2010 IEEE Intl. Conf. on Data Mining, Sydney* (IEEE, 2010), pp. 18–27.
[42] P. Bovet and S. Benhamou, Spatial analysis of animals' movements using a correlated random walk model, J. Theor. Biol. **131**, 419 (1988).
[43] C. Bélisle and J. Faraway, Winding angle and maximum winding angle of the two-dimensional random walk, J. Appl. Probab. **28**, 717 (1991).
[44] S. Obukhov and L. Peliti, Renormalisation of the 'true' self-avoiding walk, J. Phys. A: Math. Gen. **16**, L147 (1983).
[45] S. Derkachov, J. Honkonen, E. Karjalainen, and A. Vasil'ev, Renormalisability and renormalisation of the 'true' self-avoiding random walks, J. Phys. A: Math. Gen. **22**, L385 (1989).
[46] M. N. Najafi, J. Cheraghalizadeh, and H. J. Herrmann, Self-organized criticality in cumulus clouds, Phys. Rev. E **103**, 052106 (2021).